

RECONSTRUCTING COMPLEX FLUID PROPERTIES FROM THE BEHAVIOR OF FLUCTUATING IMMERSSED PARTICLES *

CHRISTEL HOHENEGGER[†] AND SCOTT A. MCKINLEY[‡]

Abstract. Complex fluids have long been characterized by two functions that summarize the fluid’s elastic and viscous properties, respectively called the storage ($G'(\omega)$) and loss ($G''(\omega)$) moduli. A fundamental observation in this field, which is called *passive microrheology* is that information about these bulk fluid properties can be inferred from the path statistics of immersed, fluctuating microparticles. In this work, we perform a systematic study of the multi-step protocol that forms the foundation of this field. Particle velocities are assumed to be well-described by the Generalized Langevin Equation, a stochastic integro-differential equation uniquely characterized by a memory kernel $G_r(t)$, which is hypothesized to be inherited from the surrounding fluid. We establish rigorous justification for a key relationship between a particle’s Mean Squared Displacement and its memory kernel $G_r(t)$, but simultaneously show that the justification used in the literature for the last fifty years is not actually true. With this foundation in hand, by way of a tunable four-parameter family of functions that can serve as particle memory functions, we analyze errors and uncertainties intrinsic in passive microrheology techniques. We show that, despite the fact that certain parameters are essentially unidentifiable on their own, the protocol is remarkably effective in reconstructing $G'(\omega)$ and $G''(\omega)$ in a range that corresponds to the experimentally observable regime.

Key words. Microrheology, Generalized Langevin Equation, Complex Fluids, Inference

1. Introduction. *Rheology* is the study of the flow and deformation of soft matter, especially in response to applied forces. For materials ranging from polymer melts to cake batter, the theory of rheology has provided insight and a common language for describing both the fluid-like and solid-like properties of complex fluids [20]. Traditionally, the experiments that assess these properties require liters of material, but this poses a serious problem when investigating biological materials. While there is no problem producing liters to sample for many materials used in industry, this is simply not possible for biological fluids like mucus and cytoplasm. The advent of nano-scale single particle tracking opened the way for new modes of investigation. In their seminal paper, Mason & Weitz [23] were able to relate the statistics of individual particle paths with bulk fluid properties. Over the last twenty years, there have been numerous modifications and extensions to the theory [24, 33, 34, 21, 13, 3], which has become a vital tool for investigating characterizing healthy and unhealthy mucus, blood, and various biofilms [35, 1, 25, 18, 19, 2].

While the theory has been validated in some special cases, it is important to note that most inference protocols involve either (1) numerical computation of Laplace transforms, or (2) fitting of power laws on log-log plots [24, 5]. Both of these methods are notoriously noisy and should give us pause to wonder what degree of error they induce. Moreover, while data is collected in the time domain, rheological properties are expressed in frequency space. When experiments are constrained by a camera’s frame rate, on the one hand, and the tendency to diffuse out of a field of view, on the other, it is not immediately clear what the bound of accurate inference will be on the frequency side. These concerns call for a rigorous investigation into the intrinsic uncertainty that arises from the chain of assumptions that constitute a standard microrheological protocol. In this work, we provide such an investigation, demonstrating

*Submitted to the editors May 2017.

Funding: The authors were supported by NSF-DMS 1412998.

[†]Department of Mathematics, University of Utah, Salt Lake City, UT (choheneg@math.utah.edu).

[‡]Department of Mathematics, Tulane University, New Orleans, LA (scott.mckinley@tulane.edu).

both strengths and weaknesses that exist in the current paradigm.

1.1. Bulk Fluid Properties. The linear response of a viscoelastic medium to a shear force is summarized by its shear relaxation modulus $G_r(t)$, which is used to relate a fluid's stress response $\sigma(t)$ to an applied shear rate $\dot{\gamma}(t)$. A one-dimensional version of such a *constitutive equation* is

$$(1) \quad \sigma(t) = \int_0^t G_r(t-t') \dot{\gamma}(t') dt'.$$

It has been experimentally observed that when an oscillatory shear, $\gamma(t) = \gamma_0 \sin(\omega t)$, is applied to a complex fluid, the stress response will also be oscillatory, but possibly out of phase:

$$(2) \quad \begin{aligned} \sigma(t) &= \sigma_0 \sin(\omega t + \phi(\omega)) \\ &= \sigma_0 \cos(\phi(\omega)) \sin(\omega t) + \sigma_0 \sin(\phi(\omega)) \cos(\omega t). \end{aligned}$$

A pure solid will respond in phase, $\phi(t) \equiv 0$, while a viscous fluid will respond out of phase with $\phi(t) \equiv \pi/2$. In general, the phase of the stress response will be ω -dependent. The coefficient of $\sin(\omega t)$ is considered the ω -dependent magnitude of the elastic response, while the coefficient of $\cos(\omega t)$ is the magnitude of the viscous response.

The stress can also be expressed in terms of the shear relaxation modulus $G_r(t)$ and the rate of strain $\dot{\gamma}(t) = \gamma_0 \omega \cos(\omega t)$ through the constitutive equation (1):

$$(3) \quad \begin{aligned} \sigma(t) &= \int_0^t G_r(t-t') \gamma_0 \omega \cos(\omega t') dt' \stackrel{(u=t-t')}{=} \gamma_0 \omega \int_0^t G_r(u) \cos(\omega(t-u)) du \\ &= \gamma_0 \omega \int_0^t G_r(u) (\sin(\omega t) \sin(\omega u) + \cos(\omega t) \cos(\omega u)) du \\ &= \gamma_0 \omega \left(\int_0^t G_r(u) \sin(\omega u) du \right) \sin(\omega t) + \gamma_0 \omega \left(\int_0^t G_r(u) \cos(\omega u) du \right) \cos(\omega t). \end{aligned}$$

Comparing the coefficients of $\sin(\omega t)$ and $\cos(\omega t)$ in Equations 2 and 3, we see that the elastic and the viscous components of the response can be represented through the Fourier sine and cosine transforms of $G_r(t)$. These are respectively called the *shear storage modulus* $G'(\omega)$ and the *shear loss modulus* $G''(\omega)$ [20]:

$$(4) \quad \begin{aligned} \text{Storage: } G'(\omega) &:= \omega \int_0^\infty G_r(t) \sin(\omega t) dt \\ \text{Loss: } G''(\omega) &:= \omega \int_0^\infty G_r(t) \cos(\omega t) dt \end{aligned}$$

We note that the use of “primes” in the names G' and G'' is a notational idiom from the rheology literature and does not imply that we are taking derivatives of a function G .

For a purely viscous fluid, the response to shear is instantaneous, so $G_r(t)$ is a Dirac δ -function. In turn, the storage and loss moduli are $G'(\omega) = 0$ and $G''(\omega) = \eta_s \omega$. The relaxation modulus can take on many forms for viscoelastic fluids, but an important class, which we refer to as *generalized Maxwell fluids with intrinsic viscosity*, consists of a Dirac δ -function linearly superimposed with a collection of exponential

decay functions called *Maxwell elements*:

$$(5) \quad \text{Viscoelastic Relaxation: } G_r(t) = \eta_s \delta(t) + \sum_{n=1}^N G_n e^{-t/\tau_n} 1_{\{t \geq 0\}}.$$

The positive values $\{\tau_n\}$ are called *relaxation times*. The values $\{G_n\}$ are also positive and have units of [pressure]. We use $1_{t \geq 0}$ to denote the unit step function. Throughout this work, we will focus on a special structure, which has been called the *generalized Rouse relaxation spectrum*. See Eq. (2.1) for the definition below. The storage and loss moduli are in turn often summarized by the so-called *complex modulus* $G^*(\omega)$, which is defined to be

$$(6) \quad G^*(\omega) := G'(\omega) + iG''(\omega).$$

The complex modulus is related to what is called the *complex viscosity* through the formula $\eta^*(\omega) := G^*(\omega)/i\omega$. By a formal calculation using the definitions of the Fourier transform and of the Fourier sine and cosine transforms, it follows that $\eta^*(\omega) = \widehat{G}_r(\omega)$, where $\widehat{\cdot}$ denotes the Fourier transform. As a consequence of the definition (5), we have that $\tilde{\eta}(s) = \widetilde{G}_r(s)$, where $\tilde{\cdot}$ denote the (unilateral) Laplace transform.

Examples of the shear storage and shear loss moduli for the Generalized Rouse Kernel considered in this work are provided in Figure 1 as a function of the number of Maxwell elements and of the subdiffusive exponent. The asymptotic behavior near zero is such that $G'(\omega)$ is quadratic (slope 2 on a log-log plot) and $G''(\omega)$ is linear (slope 1 on a log-log plot). For large ω , $G'(\omega)$ is constant, while $G''(\omega)$ grows linearly. The length of the transition region is a function of both the subdiffusive exponent and the number of Maxwell elements.

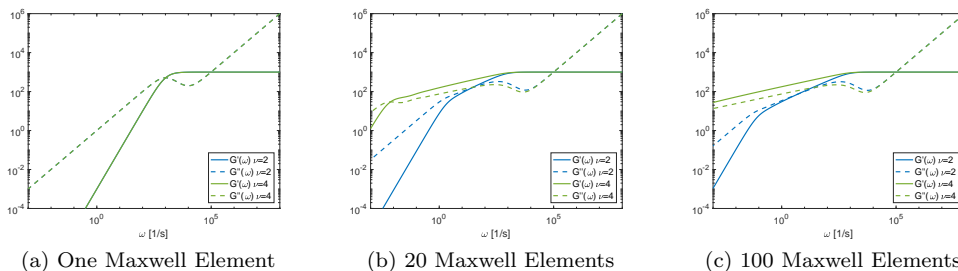


FIG. 1. STORAGE AND LOSS MODULI FOR GENERALIZED ROUSE KERNEL as a function of the number of Maxwell elements. The smallest relaxation time is $\tau_0 = 10^{-3}$ s, the solvent viscosity is $\eta_s = 10^{-2}$ g/(cm s) and the ratio η_p/τ_{avg} is the same independently of the number of kernels, here $\eta_p/\tau_{avg} = 10^3$ g/(cm s²). The green curves corresponds to a subdiffusive exponent $\nu = 4$, while the blue curves are obtained with $\nu = 2$.

1.2. Passive Microrheology. Let $(X(t))_{t \geq 0}$ denote the position of a particle at time t and let $(V(t))_{t \geq 0}$ denote its velocity. The classical model for the velocity of a particle in a viscous fluid is the Langevin Equation:

$$(7) \quad \text{Langevin Equation} \\ \overline{m}dV(t) = -\gamma V(t)dt + \sqrt{2k_B T \gamma} dW(t),$$

where m is the mass of the particle, k_B is Boltzmann constant, T is the temperature of the system, γ is the drag coefficient and $W(t)$ is a standard Brownian motion. By Stokes Law, if the particle is a sphere of radius a and the fluid has viscosity η_s , then $\gamma = 6\pi a\eta_s$.

Using standard Stochastic Calculus, one can show that

$$(8) \quad \lim_{t \rightarrow \infty} \frac{1}{t} \mathbb{E}(|X(t)|^2) = \frac{dk_B T}{3\pi a\eta_s},$$

where d is the number of observed dimensions. This establishes the fundamental Stokes-Einstein relationship between the viscosity of a fluid and the Mean Squared Displacement (MSD), $M(t) := \mathbb{E}(|X(t)|^2)$ of an immersed particle.

Intrinsic in the development of the Langevin Equation is the assumption that the diffusing particle of interest is much larger than the particles in the fluid environment that collide with it generating both drag and thermal excitation. For this reason, the Generalized Langevin Equation (GLE) was introduced by H. Mori [27] and R. Kubo [16, 15], and soon thereafter R. Zwanzig & M. Bixon [37] proposed that the Stokes-Einstein relationship could be generalized for simple viscoelastic fluids. It would be another 25 years though, before a fully realized connection between viscoelastic diffusion and the GLE was proposed. In their seminal work, T.G. Mason & M.A. Weitz [23] hypothesized that the drag force experienced by a particle immersed in a viscoelastic fluid is directly proportional to the shear relaxation modulus $G_r(t)$:

Generalized Langevin Equation (Informal Definition)

$$(9) \quad m\dot{V}(t) = -6\pi a \int_{-\infty}^t G_r(t-s)V(s)ds + F(t)$$

where $F(t)$ is a mean-zero, stationary, Gaussian process with an autocovariance function defined so that the velocity process satisfies the equipartition theorem [32]

$$(10) \quad m\mathbb{E}(|V(0)|^2) = dk_B T.$$

If $G_r(t)$ is purely viscous, i.e. $G_r(t) = \eta_s\delta(t)$, then we recover the Langevin Equation. By way of a formal argument using Laplace Transforms, Mason & Weitz were the first to establish a relationship between the Laplace Transform of a fluid's relaxation modulus $\tilde{G}_r(s)$ and that of an immersed particle's MSD.

In practice, MSD is computed path-by-path. Assuming that the j th particle has been observed for N steps uniformly separated by time intervals of length δ , we define

$$(11) \quad \mathcal{M}_j(n\delta) := \frac{1}{N-n+1} \sum_{k=0}^{N-n} |X_j((n+k)\delta) - X_j(k\delta)|^2.$$

When there is no subscript denoting the particle index, we are referring to the ensemble average of J distinct particle paths:

$$(12) \quad \mathcal{M}(t) := \frac{1}{J} \sum_{j=1}^J \mathcal{M}_j(t), \text{ where } t \in \{0, \delta, 2\delta, \dots, N\delta\}.$$

We assume linear interpolation for all other t .

This completes the chain of connections that form the basis for passive microrheology, which we summarize as follows:

Passive Microrheology

$$(13) \quad \mathcal{M}(t) \longleftrightarrow M(t) \xleftrightarrow{GLE} \tilde{G}_r(s) \longleftrightarrow (G'(\omega), G''(\omega)).$$

There are multiple proposals for how to approximate and/or efficiently compute each of the \longleftrightarrow connections, each introducing another layer of uncertainty.

In what follows, we assume a particular form for the relaxation modulus that depends on four parameters and allows for an incremental interpolation between the viscous and viscoelastic regimes. In Section 2, we rigorously establish a sequence of essential properties of the GLE. Theorem 2.4, in particular, is essential for reconstruction of fluid properties from path data. Interesting, the “proof” that has appeared in the physics literature rests on an assumption that we can show is not true, Theorem 2.5. Nevertheless, the protocol in used in practice is theoretically sound and we proceed in Section 3 to characterize the degree of error that is introduced by each link in the chain (13). We seek to characterize the degree of uncertainty that arises from each step, first assuming perfect knowledge of $\tilde{G}_r(s)$ and then analyzing the impact of limited observations. The theme that arises throughout the analysis is that, while there is significant error in the estimation of individual parameters, the reconstruction of $G'(\omega)$ and $G''(\omega)$ is remarkably robust in the frequency range that corresponds to the time domain observation window.

2. Generalized Langevin Equation. In this section, we lay out some basic properties of the GLE. For simplicity we assume that $X(t)$ refers to a particle’s x -coordinate and so all processes below are one-dimensional.

Generalized Langevin Equation

$$(14) \quad mdV(t) = (-\gamma V(t) - \beta(K^+ * V)(t) + \sqrt{c\beta}F(t))dt + \sqrt{2c\gamma}dW(t)$$

where $K \in L^1(\mathbb{R})$ is positive definite, $K^+(t) := K(t)1_{t \geq 0}$, $*$ denotes the convolution, and defining $\|K^+\|_1 := \int_{\mathbb{R}} |K^+(t)|dt$,

$$(15) \quad \gamma = 6\pi a\eta_s, \quad \beta = \frac{6\pi a\eta_p}{\|K^+\|_1}, \quad \text{and } c = k_B T.$$

This is the velocity process associated with the shear relaxation modulus

$$(16) \quad G_r(t) = \eta_s \delta(t) + \frac{\eta_p}{\|K^+\|_1} K^+(t).$$

Meanwhile $F(t)$ is a stationary, mean-zero, Gaussian process satisfying

$$(17) \quad \mathbb{E}(F(t)F(s)) = K(t-s).$$

When K can be expressed as a sum of exponential functions, we say it is in the Prony series class:

$$(18) \quad \mathcal{H}_{\text{Prony}} := \left\{ K : K(t) = \sum_{n=0}^{N-1} G_n e^{-|t|/\tau_n}, \text{ where } G_n, \tau_n > 0 \text{ for all } n \right\}.$$

We will typically work with a subset of the Prony series class called the generalized Rouse kernels.

DEFINITION 2.1. We say that $K \in \mathcal{K}_{\text{Rouse}}$ if for some $N \in \mathbb{N}$, $\nu \geq 1$ and $\tau_0 > 0$, we have

$$(19) \quad K(t) = \frac{1}{N} \sum_{n=0}^{N-1} e^{-|t|/\tau_n}, \text{ where } \tau_n = \tau_0 \left(\frac{N}{N-n} \right)^\nu.$$

We call $\{\tau_n\}_{n=0}^{N-1}$ the generalized Rouse spectrum of relaxation times with shape parameter ν .

Note that when $K \in \mathcal{K}_{\text{Rouse}}$, $\|K^+\|_1 = \langle \tau_n \rangle := (\sum_n \tau_n)/N$.

THEOREM 2.2. Suppose that $K \in \mathcal{K}_{\text{Prony}}$. Then there exists a Gaussian, mean-zero, stationary process $V(t)$ satisfying the GLE (14), and it has the spectral density

$$(20) \quad \widehat{\rho}(\omega) = \frac{2c\gamma + k_B T \beta \widehat{K}(\omega)}{|mi\omega + \gamma + \beta \widehat{K}^+(\omega)|^2}.$$

Moreover, the sample paths of V are continuous almost surely and $\mathbb{E}(V(0)^2) = k_B T/m$.

Proof. The construction of the solution and almost sure continuity are established in [28]. If K is a sum of exponentials, then existence and regularity was established in [7] and the proof that equipartition of energy (Equation 10) is satisfied is given in [12] and [10]. \square

Using ϖ to denote elements of the probability space $(\Omega, \mathcal{F}, \mathbb{P})$ on which V is defined, let Ω_c be the probability one event such that for all $\varpi \in \Omega_c$, $(V(t; \varpi))_{t \in \mathbb{R}}$ is continuous. For $t \geq 0$, define $X(t)$ by

$$(21) \quad X(t; \varpi) := \begin{cases} \int_0^t V(t'; \varpi) dt', & \varpi \in \Omega_c \\ 0, & \text{otherwise.} \end{cases}$$

The dynamics of a single-mode Maxwell model are described at length by Grimm et al. [8]. While there is a nonlinear feature in the MSD of the position process for such a process, it has been established that *many* modes are necessary to produce persistent anomalous subdiffusive behavior [17, 14, 26]. However, if there are finitely many modes, the MSD is always eventually linear so we call such behavior *transient anomalous diffusion*. This can be rigorously stated as follows. (See [28] for proof).

THEOREM 2.3 (Transient Anomalous Diffusion). Let $M(t) := \mathbb{E}(X^2(t))$ be the MSD of $(X(t))_{t \geq 0}$. Then for all $K \in \mathcal{K}_{\text{Prony}}$, the associated particle process $(X(t), V(t))$ has MSD $M(t) := \mathbb{E}(X^2(t))$ satisfying

$$(22) \quad \lim_{t \rightarrow \infty} \frac{M(t)}{t} = C \in (0, \infty).$$

However, suppose that the sequence of particle processes $\{X_N(t), V_N(t)\}_{N \in \mathbb{N}}$ have memory kernels $\{K_N\}_{N \in \mathbb{N}} \subset \mathcal{K}_{\text{Rouse}}$ respectively with N terms and common parameters $\tau_0 > 0$ and $\nu > 1$. Then, denoting $M_N(t) = \mathbb{E}(X_N^2(t))$, there exists a function $f(t)$ satisfying

$$(23) \quad \lim_{t \rightarrow \infty} f(t) t^{-\frac{1}{\nu}} = C' \in (0, \infty)$$

such that for all $T > 0$,

$$(24) \quad \lim_{N \rightarrow \infty} \sup_{t \in [0, T]} |M_N(t) - f(t)| = 0.$$

With this backdrop, we proceed to the primary mathematical contributions of this manuscript. First, in Theorem 2.4, we validate the fundamental formula in passive microrheology that relates the Laplace transform of a particle's MSD to its shear relaxation modulus. We then proceed in Theorem 2.5 to comment on a property that has long been assumed to be true in the physics literature, but is not, in fact true.

THEOREM 2.4 (The connection $M(t) \longleftrightarrow \tilde{G}_r(s)$). *Let $((X(t), V(t)))_{t \geq 0}$ be a particle process with shear relaxation modulus $G_r(t)$ of the form (16) that has a memory kernel $K \in \mathcal{K}_{\text{Prony}}$. Let $\tilde{M}(s)$ to be the Laplace transform of the associated MSD. Then*

$$(25) \quad 6\pi a \tilde{G}_r(s) = \frac{2c}{s^2 \tilde{M}(s)} - ms.$$

Proof. In order to prove this theorem, we will adopt an alternative Markovian form of the GLE that relies on introducing auxiliary variables. Such an approach was pioneered by Mori [27] and Zwanzig [36] and was used more recently for the GLE by Fricks et al [7] and McKinley et al [26]. The form presented here is derived from Pavliotis [30]. Suppose that K is a sum of n exponentials. For clearer exposition, define $\lambda_n = \tau_n^{-1}$ for each $n \in \{0, \dots, N-1\}$ and consider the system of SDEs:

$$(26) \quad \begin{aligned} mdV(t) &= -\gamma V(t) - \sum_n \sqrt{\beta G_n} Z_n dt + \sqrt{2c\gamma} dW(t); \\ dZ_n(t) &= -\lambda_n Z_n(t) + \sqrt{\beta G_n} V(t) dt + \sqrt{2c\lambda_n} dW_n(t). \end{aligned}$$

By the same argument presented in Pavliotis, Ch 8 [30], the $V(t)$ defined here is equivalent in distribution to the definition (14). Similar to the form presented by Pavliotis, we claim that

$$(27) \quad p(v, \mathbf{z}) := C \exp\left(-\frac{1}{2c}(mv^2 + |\mathbf{z}|^2)\right)$$

is the stationary distribution of the system (26). To prove this, note that the operator \mathcal{L} associated with this system of SDEs acts on a function $f(v, \mathbf{z})$ that is twice continuously differentiable in all its variables as follows:

$$\begin{aligned} \mathcal{L}f(v, \mathbf{z}) &= -\left(\frac{\gamma}{m}v + \frac{\sqrt{\beta}}{m} \sum_n \sqrt{G_n} z_n\right) \frac{\partial f}{\partial v} + \frac{c\gamma}{m^2} \frac{\partial^2 f}{\partial v^2} \\ &\quad + \sum_n (\lambda_n z_n + \sqrt{\beta G_n} v) \frac{\partial f}{\partial z_n} + c\lambda_n \frac{\partial^2 f}{\partial z_n^2}. \end{aligned}$$

Then, one can show that $p(v, \mathbf{z})$ is the stationary distribution by checking that $\mathcal{L}^*p = 0$, where \mathcal{L}^* is the adjoint of \mathcal{L} , satisfying

$$(28) \quad \begin{aligned} \mathcal{L}^*p(v, \mathbf{z}) &= \frac{\partial}{\partial v} \left(\left(\frac{\gamma}{m}v + \sum_n \frac{\sqrt{\beta G_n}}{m} z_n \right) p(v, \mathbf{z}) \right) + \frac{c\gamma}{m^2} \frac{\partial^2 p(v, \mathbf{z})}{\partial v^2} \\ &\quad + \sum_n \frac{\partial}{\partial z_n} \left(\left(\lambda_n z_n + \sqrt{\beta G_n} v \right) p(v, \mathbf{z}) \right) + c\lambda_n \frac{\partial^2 p(v, \mathbf{z})}{\partial z_n^2}. \end{aligned}$$

If the initial condition $(V(0), \mathbf{Z}(0))$ is drawn from the stationary distribution, note

that the product structure of $p(v, \mathbf{z})$ yields

$$(29) \quad \begin{aligned} \mathbb{E}(V(0)Z_n(0)) &= \int_{\mathbb{R}^{n+1}} v z_n p(v, \mathbf{z}) dv d\mathbf{z} \\ &= C \int_{\mathbb{R}} v e^{-\frac{mv^2}{2c}} dv \int_{\mathbb{R}} z_n e^{-\frac{z_n^2}{2c}} dz_n \prod_{m \neq n} \left(\int_{\mathbb{R}} e^{-\frac{z_m^2}{2c}} dz_m \right) = 0. \end{aligned}$$

Now, recalling the definition $\rho(t) := \mathbb{E}(V(t)V(0))$ and introducing $\rho_n(t) := \mathbb{E}(Z_n(t)V(0))$, we can multiply (26) through by $V(0)$ and take expectations, resulting in the following system of ODEs:

$$(30) \quad m\dot{\rho}(t) = -\gamma\rho(t) - \sum_n \sqrt{\beta G_n} \rho_n(t)$$

$$(31) \quad \dot{\rho}_n(t) = -\lambda_n \rho_n(t) + \sqrt{\beta G_n} \rho(t).$$

Taking the Laplace transform of (31) yields the solution

$$\tilde{\rho}_n(s) = \frac{\tilde{\rho}(s) + \rho_n(0)}{s + \lambda_n}$$

But from (29), we have that $\rho_n(0) = 0$. Moreover, from Theorem 2.2, $\rho(0) = c/m$. Therefore, substituting what remains in (30), we find that

$$(32) \quad \tilde{\rho}(s) = \frac{m\rho(0)}{ms + \gamma + \sum_n \beta G_n \frac{1}{s + \lambda_n}} = \frac{c}{ms + 6\pi a \tilde{G}_r(s)}$$

To complete the proof we note that $\rho(t)$ is related to the MSD by way of the relation

$$(33) \quad M(t) = 2 \int_0^t (t - t') \rho(t') dt'.$$

This equation appears in Reif, Chapter 15 [32] for example. It follows that $\tilde{\rho}(s) = s^2 \tilde{M}(s)/2$. Equation 25 follows immediately. \square

2.1. A comment on $\mathbb{E}(F(t)V(0))$. In order to derive the relationship between the shear relaxation modulus and the MSD (Theorem 2.4), arguments in the physics literature typically rely on an assumption that turns out not to be true.

In Mason & Weitz [23], Mason [24], and Squires [33], we note that the GLE is defined slightly differently than the informal version of the GLE we presented in Equation 9. The lower limit of integration for the convolution term is zero in these references, rather than negative infinity. The authors formally multiply through by $V(0)$ and take expectations. The claim is then that $\rho(t) := \mathbb{E}(V(t)V(0))$ must satisfy the integro-differential equation

$$\text{Mason \& Weitz [23]:} \quad m\dot{\rho}(t) = -6\pi a \int_0^t G_r(t - t') \rho(t') dt' + \mathbb{E}(F(t)V(0)).$$

Applying the Laplace transform, the authors solve for $\tilde{\rho}(s)$,

$$\tilde{\rho}(s) = \frac{m\rho(0)}{ms + 6\pi a \tilde{G}_r(s)} + \frac{\mathcal{L}[\mathbb{E}(F(t)V(0))](s)}{ms + 6\pi a \tilde{G}_r(s)}$$

Then, it is generally *assumed* that $\mathbb{E}(F(t)V(0)) = 0$ for all t so that the last term vanishes. Indeed “ $\mathbb{E}(F(t)V(0))$ ” has appeared explicitly as an assumption in Reif’s text [32], in Kubo’s paper on the Fluctuation-Dissipation Theorem [16], in Mason & Weitz [23] and Mason [24], and in Squires review on microrheology [33]. We can use a different Markovian framework from the one used in the proof of Theorem 2.4 to show that, in fact, $\mathbb{E}(F(t)V(0)) \neq 0$.

THEOREM 2.5. *Let $((X(t), V(t)))_{t \geq 0}$ be a particle process with shear relaxation modulus $G_r(t)$ of the form (16) that has a memory kernel $K \in \mathcal{K}_{Prony}$. If $V(t)$ is a stationary solution to (14), then*

$$(34) \quad \mathbb{E}(F(t)V(0)) = \sum_{n=0}^{N-1} \frac{G_n \sqrt{\beta c}}{m\tau_n^{-1} + 6\pi a \tilde{G}_r(\tau_n^{-1})} e^{-t/\tau_n}.$$

Proof. Again, for cleaner exposition, let $\lambda_n := \tau_n^{-1}$. For each n , define

$$(35) \quad Z_n(t) := \int_{-\infty}^t e^{-\lambda_n(t-t')} V(t') dt'.$$

Then the GLE can be rewritten as a system of SDEs (all sums in what follows range over $n \in \{0, \dots, N-1\}$):

$$(36) \quad \begin{aligned} mdV(t) &= \left(-\gamma V(t) - \beta \left(\sum_n G_n Z_n \right) + \sqrt{c\beta} \left(\sum_n \sqrt{G_n} F_n \right) \right) dt + \sqrt{2c\gamma} dW(t); \\ dZ_n(t) &= -\lambda_n Z_n(t) + V(t) dt; \\ dF_n(t) &= -\lambda_n F_n(t) + \sqrt{2\lambda_n} dW_n(t), \end{aligned}$$

where the $\{W_n(t)\}_{t \geq 0}$ are iid standard Brownian motions.

The velocity process here is equal in distribution to that of Theorem 2.4, but the Markov representation allows us to have an initial condition that is not in the stationary distribution. For example, the version of the informal GLE (9) with initial time 0 would correspond to taking $Z_n(0) = 0$ for all n , while $F_n(0)$ would be drawn from the stationary distribution (Gaussian with mean zero and variance one).

We define the following time-dependent quantities:

$$(37) \quad \rho_{z_n}(t) := \mathbb{E}(Z_n(t)V(0)), \quad \rho_{f_n}(t) := \mathbb{E}(F_n(t)V(0)),$$

and

$$(38) \quad \begin{aligned} \varphi_{vv}(t) &:= \mathbb{E}(V(t)^2); \\ \varphi_{vz_n}(t) &:= \mathbb{E}(V(t)Z_n(t)); \quad \varphi_{vf_n}(t) := \mathbb{E}(V(t)F_n(t)); \\ \varphi_{z_n z_k}(t) &:= \mathbb{E}(Z_n(t)Z_k(t)); \quad \varphi_{z_n f_k}(t) := \mathbb{E}(Z_n(t)F_k(t)); \\ \varphi_{f_n f_k}(t) &:= \mathbb{E}(F_n(t)F_k(t)). \end{aligned}$$

If we multiply (36) through by $V(0)$ and take expectations, we have the system of ODEs

$$(39) \quad \begin{aligned} m\dot{\rho}(t) &= -\gamma\rho(t) - \beta \left(\sum_n G_n \rho_{z_n}(t) \right) + \sqrt{c\beta} \left(\sum_n \sqrt{G_n} \rho_{f_n}(t) \right) \\ \dot{\rho}_{z_n}(t) &= -\lambda_n \rho_{z_n}(t) + \rho(t) \\ \dot{\rho}_{f_n}(t) &= -\lambda_n \rho_{f_n}(t) \end{aligned}$$

Note that the Laplace transforms of the latter two equations can be written in the form

$$(40) \quad \tilde{\rho}_{z_n}(s) = \frac{\tilde{\rho}(s) + \varphi_{vz_n}(0)}{s + \lambda_n} \text{ and } \tilde{\rho}_{f_n}(s) = \frac{\varphi_{vf_n}(0)}{s + \lambda_n}.$$

Recalling that $\widetilde{K^+}(s) = \sum_n G_n / (s + \lambda_n)$, we find that

$$(41) \quad \tilde{\rho}(s) = \frac{m\rho(0)}{ms + \gamma + \beta\widetilde{K^+}(s)} + \sum_n \frac{-\beta G_n \varphi_{vz_n}(0) + \sqrt{c\beta G_n} \varphi_{vf_n}(0)}{(ms + \gamma + \beta\widetilde{K^+}(s))(s + \lambda_n)}.$$

From Equation 32 in the proof of Theorem 2.4, we know that the sum must be zero. In fact, something stronger is true. Each summand is zero. To prove this, it suffices to show that the stationary system satisfies the following claim,

$$(42) \quad \text{Auxiliary Balance Condition: } \beta G_n \bar{\varphi}_{vz_n} = \sqrt{c\beta G_n} \bar{\varphi}_{vf_n} \text{ for all } n,$$

where we have introduced the $\bar{\varphi}_{[\dots]} := \varphi_{[\dots]}(0)$ when the system has initial condition drawn from the stationary distribution.

In order to analyze the covariation of the auxiliary variables, suppose for a moment that we do not start in the stationary distribution. Applying Itô's formula to each product in the system of equations (38) and taking expectations yields the following system of ordinary differential equations,

$$(43) \quad \frac{m}{2} \dot{\varphi}_{vv} = -\gamma \varphi_{vv} + \frac{c\gamma}{m} + \sum_n \left(-\beta G_n \varphi_{vz_n} + \sqrt{c\beta G_n} \varphi_{vf_n} \right);$$

$$(44) \quad m \dot{\varphi}_{vz_n} = -(m\lambda_n + \gamma) \varphi_{vz_n} + m \varphi_{vv} + \sum_k \left(-\beta G_k \varphi_{z_n z_k} + \sqrt{c\beta G_k} \varphi_{z_n f_k} \right);$$

$$(45) \quad m \dot{\varphi}_{vf_n} = -(m\lambda_n + \gamma) \varphi_{vf_n} + \sum_k \left(-\beta G_k \varphi_{z_k f_n} + \sqrt{c\beta G_k} \varphi_{f_n f_k} \right);$$

$$(46) \quad \dot{\varphi}_{z_n z_k} = -(\lambda_n + \lambda_k) \varphi_{z_n z_k} + (\varphi_{vz_n} + \varphi_{vz_k});$$

$$(47) \quad \dot{\varphi}_{z_n f_k} = -(\lambda_n + \lambda_k) \varphi_{z_n f_k} + \varphi_{vf_k};$$

$$(48) \quad \dot{\varphi}_{f_n f_k} = -(\lambda_n + \lambda_k) \varphi_{f_n f_k} + 2\lambda_n \delta_{nk}.$$

where, in Equation 48, δ_{nk} is the Kronecker δ -function. For each pair, the stationary covariance can be obtained by taking $\bar{\varphi}_{[\dots]} = \lim_{t \rightarrow \infty} \varphi_{[\dots]}(t)$, or by setting all derivatives on the left-hand side to zero and solving the resulting set of linear equations. We take the latter approach.

Recall first that, by Theorem 2.2, $m\bar{\varphi}_{vv} = c$. This cancels the first two terms of the steady-state version of (43). What remains is exactly the Auxiliary Balance Condition (42).

Next, we note that (48) is autonomous so

$$(49) \quad \bar{\varphi}_{f_n f_k} = \delta_{nk}.$$

From (47) and (46) we see that

$$(50) \quad \bar{\varphi}_{z_n f_k} = \frac{1}{\lambda_n + \lambda_k} \bar{\varphi}_{vf_k} \text{ and } \bar{\varphi}_{z_n z_k} = \frac{1}{\lambda_n + \lambda_k} (\bar{\varphi}_{vz_n} + \bar{\varphi}_{vz_k}).$$

Substituting the first relation from (50) and (49) into (45) we have

$$(m\lambda_n + \gamma)\bar{\varphi}_{vf_n} = \sum_k \left(-\frac{\beta G_k}{\lambda_n + \lambda_k} \bar{\varphi}_{vf_n} + \sqrt{c\beta G_k} \delta_{nk} \right),$$

which simplifies to

$$(51) \quad (m\lambda_n + \gamma + \beta \tilde{K}^+(\lambda_n)) \bar{\varphi}_{vf_n} = \sqrt{c\beta G_n}.$$

It remains to solve for $\bar{\varphi}_{vz_n}$ and note that when compared to (51), the Auxiliary Balance Condition holds. Indeed, substituting the second relation from (50) into (44) and again using $m\bar{\varphi}_{vv} = c$, we have

$$(m\lambda_n + \gamma)\bar{\varphi}_{vz_n} = c + \sum_k \left(-\frac{\beta G_k(\bar{\varphi}_{vz_n} + \bar{\varphi}_{vz_k})}{\lambda_n + \lambda_k} + \frac{\sqrt{c\beta G_k} \bar{\varphi}_{vf_k}}{\lambda_n + \lambda_k} \right)$$

which, using the Auxiliary Balance Condition, simplifies to

$$(52) \quad (m\lambda_n + \gamma + \beta \tilde{K}^+(\lambda_n)) \bar{\varphi}_{vz_n} = c$$

Therefore the Auxiliary Balance Condition is consistent and, to summarize, the covariances of the stationary distribution satisfy

$$(53) \quad \begin{aligned} \bar{\varphi}_{vv} &= c/m; & \bar{\varphi}_{f_n f_k} &= \delta_{nk}; \\ \bar{\varphi}_{vz_n} &= c/(m\lambda_n + \gamma + \beta \tilde{K}^+(\lambda_n)); \\ \bar{\varphi}_{vf_n} &= \sqrt{c\beta G_n}/(m\lambda_n + \gamma + \beta \tilde{K}^+(\lambda_n)); \\ \bar{\varphi}_{z_n z_k} &= (\bar{\varphi}_{vz_n} + \bar{\varphi}_{vz_k})/(\lambda_n + \lambda_k); \\ \bar{\varphi}_{z_n f_k} &= \bar{\varphi}_{vf_k}/(\lambda_n + \lambda_k). \end{aligned}$$

Finally, recalling from Equation 36 that $F(t) = \sum_n \sqrt{G_n} F_n$, and we find from Equation 40 that

$$\mathcal{L}\{\mathbb{E}(F(t)V(0))\}(s) = \sum_n \sqrt{G_n} \frac{\varphi_{vf_n}}{s + \lambda_n},$$

from which (34) follows. \square

3. Parameter Estimation and a Monte Carlo Visualization of Uncertainty for Rheological Properties.

3.1. Parametric Inference Imposes Small- and Large- ω Asymptotics.

For the work we present in this section, we work within the $\mathcal{K}_{\text{Prony}}$ framework for modeling viscoelastic diffusion. It is important to note that this imposes a structure on the storage and loss moduli G' and G'' .

PROPOSITION 3.1. *Let $K \in \mathcal{K}_{\text{Prony}}$. Then the storage and loss moduli have the following asymptotic properties:*

$$(54) \quad \lim_{\omega \rightarrow 0} \frac{G'(\omega)}{\omega^2} = \frac{\eta_p \langle \tau_n^2 \rangle}{\langle \tau_n \rangle}; \quad \lim_{\omega \rightarrow \infty} G'(\omega) = \frac{\eta_p}{\langle \tau_n \rangle};$$

$$(55) \quad \lim_{\omega \rightarrow 0} \frac{G''(\omega)}{\omega} = \eta_s + \frac{\eta_p}{\langle \tau_n \rangle}; \quad \lim_{\omega \rightarrow \infty} \frac{G''(\omega)}{\omega} = \eta_s.$$

where we adopt the notation

$$(56) \quad \langle \tau_n^p \rangle := \sum_{n=0}^{N-1} G_n \tau_n^p$$

where $p > 0$.

Proof. If $K \in \mathcal{K}_{\text{Prony}}$, then

$$(57) \quad \widehat{K^+}(\omega) = \sum_n \frac{G_n \tau_n}{1 + i\omega \tau_n}.$$

From the definitions of the storage and loss moduli (4), and the definition of G_r (16), we have

$$(58) \quad G'(\omega) = \frac{\eta_p}{\langle \tau_n \rangle} \sum_n \frac{G_n \tau_n^2 \omega^2}{1 + \tau_n^2 \omega^2} \quad \text{and} \quad G''(\omega) = \eta_s \omega + \frac{\eta_p}{\langle \tau_n \rangle} \sum_n \frac{G_n \tau_n \omega}{1 + \tau_n^2 \omega^2}.$$

The asymptotic expressions follow immediately. \square

Once we impose the Generalized Rouse Spectrum for the memory kernel, we can describe a feature in G' and G'' that arises from the particle's transient anomalous diffusion.

PROPOSITION 3.2. *Let $\nu > 1$, $\tau_0 > 0$ and $\eta_s > 0$ be given. For each $N \in \mathbb{N}$, let $K_N(t) \in \mathcal{K}_{\text{Rouse}}$ be the associated generalized Rouse memory kernel with N exponential terms. For every $t > 0$, define $K(t) := \lim_{N \rightarrow \infty} K_N(t)$ and let G' and G'' be the storage and loss moduli associated with the memory kernel $K(t)$. Moreover, suppose that $\eta_p = \eta_p(N)$ in such a way that $\lim_{N \rightarrow \infty} \eta_p(N) / \langle \tau_n(N) \rangle = G_0 \in (0, \infty)$. Then*

$$(59) \quad \lim_{\omega \rightarrow 0} \frac{G'(\omega)}{\omega^{\frac{1}{\nu}}} = \frac{1}{\nu} G_0 \tau_0^{\frac{1}{\nu}} C_0(\nu); \quad \lim_{\omega \rightarrow \infty} G'(\omega) = G_0;$$

$$(60) \quad \lim_{\omega \rightarrow 0} \frac{G''(\omega)}{\omega^{\frac{1}{\nu}}} = \frac{1}{\nu} G_0 \tau_0^{\frac{1}{\nu}} C_1(\nu); \quad \lim_{\omega \rightarrow \infty} \frac{G''(\omega)}{\omega} = \eta_s.$$

where $C_r := \int_0^\infty \frac{u^r}{u^{1-\frac{1}{\nu}} (1+u^2)} du$.

Proof. For $G'(\omega)$ we can rewrite (58) with the generalized Rouse kernel as a Riemann Approximation to an integral and take $N \rightarrow \infty$:

$$(61) \quad \begin{aligned} G'(\omega) &= \lim_{N \rightarrow \infty} \frac{\eta_p}{\langle \tau_n \rangle} \frac{1}{N} \sum_n \frac{\tau_n^2 \omega^2}{1 + \tau_n^2 \omega^2} = G_0 \lim_{N \rightarrow \infty} \sum_n \frac{\tau_0^2 \omega^2}{\tau_0^2 \omega^2 + (n/N)^{2\nu}} \frac{1}{N} \\ &= G_0 \int_0^1 \frac{\tau_0^2 \omega^2}{\tau_0^2 \omega^2 + x^{2\nu}} dx \end{aligned}$$

After the substitution $u = x^\nu / \tau_0 \omega$, we have

$$(62) \quad G'(\omega) = \frac{G_0 (\tau_0 \omega)^{\frac{1}{\nu}}}{\nu} \int_0^{\frac{1}{\tau_0 \omega}} \frac{1}{u^{1-\frac{1}{\nu}}} \frac{1}{1+u^2} du.$$

The same procedure yields

$$\begin{aligned}
 G''(\omega) &= \eta_s \omega + \lim_{N \rightarrow \infty} \frac{\eta_p}{\langle \tau_n \rangle} \frac{1}{N} \sum_n \frac{\tau_n \omega}{1 + \tau_n^2 \omega^2} = \eta_s \omega + G_0 \int_0^1 \frac{\tau_0 \omega x^\nu}{\tau_0^2 \omega^2 + x^{2\nu}} dx \\
 (63) \quad &= \eta_s \omega + \frac{G_0 (\tau_0 \omega)^{\frac{1}{\nu}}}{\nu} \int_0^{\frac{1}{\tau_0 \omega}} \frac{u}{u^{1-\frac{1}{\nu}} (1+u^2)} du.
 \end{aligned}$$

Since both integrands are integrable over $u \in (0, \infty)$ the $\omega \rightarrow 0$ limit follows immediately.

To assess the large- ω limit, we return to (61). As ω tends to infinity, the integrand uniformly approaches the constant function one. Therefore $G'(\omega) \rightarrow G_0$ as $\omega \rightarrow \infty$. Similarly, we see that as $\omega \rightarrow \infty$, the integrand in (63) goes to zero uniformly over $x \in [0, 1]$, leaving only the term $\eta_s \omega$. \square

3.2. Current methods; reliance on power law fits. Because power laws are so apparent in pathwise MSDs computed from live data, it is perhaps natural to simply plot the averaged pathwise MSDs on a log-log scale and use linear regression to find the power law with best fit. Then, assuming the mass is negligible, one would estimate $\tilde{G}_r(s)$ through (25), setting $m = 0$. First, note that for $\alpha \in (0, 1)$, we have $\mathcal{L}\{t^\alpha\}(s) = \Gamma(1 + \alpha)s^{-(1+\alpha)}$. Then one would estimate that

$$(64) \quad M(t) = Ct^\alpha \text{ implies } \tilde{G}_r(s) \approx \frac{2k_B T}{6\pi a C \Gamma(1 + \alpha) s^{1-\alpha}}.$$

Using the relations

$$(65) \quad G'(\omega) = -\omega \text{Im}[\tilde{G}_r(i\omega)] \text{ and } G''(\omega) = \omega \text{Re}[\tilde{G}_r(i\omega)].$$

we have that

$$(66) \quad M(t) = Ct^\alpha \text{ implies } \begin{cases} G'(\omega) = C' \cos(\alpha\pi/2) \omega^\alpha \\ G''(\omega) = C' \sin(\alpha\pi/2) \omega^\alpha \end{cases}$$

where $C' = k_B T / (3\pi a C \Gamma(1 + \alpha))$.

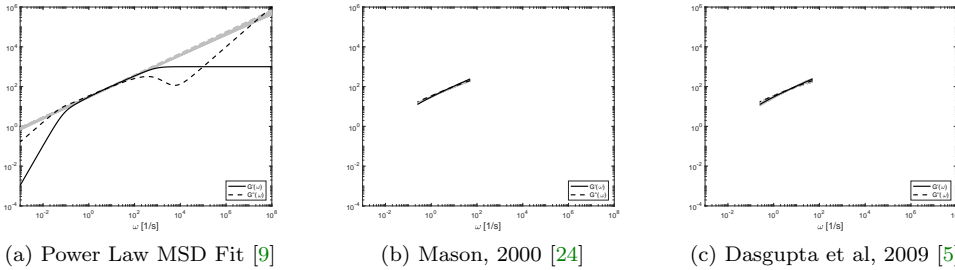


FIG. 2. ESTIMATED STORAGE AND LOSS MODULI USING EXISTING METHODS. For a fixed parameter set, we simulated 100 sets of 100 particle paths. For each set of paths, we calculated an ensemble Pathwise MSD and then applied three existing methods for inferring G' and G'' . See Sections 3.4-3.5 for further details. $N = 100$, $\tau_0 = 10^{-3} s$, $\eta_s = 10^{-2} g/(cm s)$, $\eta_p/\tau_{avg} = 10^3 g/(cm s^2)$.

As noted in Theorem 2.3, for $K \in \mathcal{K}_{\text{Rouse}}$, $\alpha = 1/\nu$. Therefore, the small- ω regime seen in (66) is the same as identified in the $N \rightarrow \infty$ limit for a generalized

Rouse kernel. In the large- ω limit, however, the $N \rightarrow \infty$ limit does not match the pure power law forms for $G'(\omega)$ and $G''(\omega)$. This is because the τ_0 is unchanged in the limit, and for all times smaller than this smallest relaxation time, the fluid is essentially viscous.

In Figure 2a, we display the results of using a pure power law fit of the MSD to infer the storage and loss moduli when the true $G_r(t)$ has a memory kernel in $\mathcal{K}_{\text{Rouse}}$ with 100 terms and $\nu = 2$. We see that the Power Law MSD fit matches the subdiffusive feature of $G'(\omega)$ and $G''(\omega)$ that appears in the range $\omega \in (10^0, 10^2) \text{ s}^{-1}$. If N were taken to be larger, the subdiffusive feature would extend in the small- ω range and presumably match the Power Law MSD fit.

In principle, a fully observed MSD will feature multiple power law regimes. For times much smaller than τ_0 the log-log slope should be one. Also, for times much larger than the largest time scale ($\sim \tau_N'$) the log-log slope will be one again. The intermediate regime of the logscale MSD will be sublinear. In their original paper on passive microrheology, Mason & Weitz computed a numerical Laplace transform of an ensemble average of Pathwise MSD curves, then used (25) to translate this to $\tilde{G}_r(s)$. They then fit to a function of the form $\tilde{G}_r(s) = a_0 + a_1s + \sum_{j=2}^J a_j s^{\nu_j}$ with $(\nu_3, \nu_4, \nu_5) = (-0.55, 0.3, 0.5)$. Invoking analytic continuation, they defined $\hat{G}_r(\omega) := \tilde{G}_r(i\omega)$ and then apply the relations (65) to compute G' and G'' . From what we have seen in (66), this imposes a small- ω form that has leading order $\omega^{-0.55}$ and a large- ω leading order ω^1 .

Concerned about the structure imposed by a parametric model for $\tilde{G}_r(s)$, Mason introduced a less-restrictive method five years later [24]. Essentially, the method is as follows. For each t , one computes a ‘‘local’’ power law fit which we denote $\alpha(t)$. Then, this is translated to an estimate for $\tilde{G}_r(s)$ using a localized version of (64):

$$(67) \quad \text{Mason, 2000 [24]:} \quad \tilde{G}_r(s) \approx \frac{2k_B T}{6\pi a s M(1/s) \Gamma(1 + \alpha(1/s))}.$$

(Note that the quantity that Mason computes ($\tilde{G}(s)$) is related to $\tilde{G}_r(s)$ by $\tilde{G}(s) = \tilde{G}_r(s)$.) The form of the approximation follows from the observation that if $M(t) = Ct^\alpha$, then the quantity $Cs^{1-\alpha}$ in the denominator of the right-hand side of (64) can be rewritten as $sM(1/s)$.

Much like the previous methods, Mason’s approximation imposes an assumption on the small- and large- ω regimes. In this case, they are set by the local power law fit and the two extremes of the observed MSD. But there is a more subtle assumption that could affect inference. While Mason’s method should be sensitive to power law transitions in the MSD form, it relies on the assumption that $\tilde{M}(s)$ can be approximated by behavior of the MSD in the neighborhood of $t = 1/s$. However, note that since $\tilde{M}(s) = \int_0^\infty M(t)e^{-st}$, its value is informed by the values of $M(t)$ in a neighborhood of the maximum value of the integrand, $t_*(s) = \arg \max_{t>0} \{M(t)e^{-st}\}$. In particular, if $M(t) = Ct^\alpha$, then $t_*(s) = \alpha/s$. In questions of interest, α is much smaller than one, meaning that Mason’s approximation samples a region of M far from the peak of the integrand’s contribution. For the same 100 sets of 100 paths, we applied Mason’s method to estimate G' and G'' . The results are displayed in Figure 2b. We only include values $\{\omega_k\}_{k=1}^{T_N}$ that are of the form $\omega_k = 1/t_k$ where t_k is a time point for which path observations were made.

For observed MSD that is highly curved, Dasgupta *et al.* proposed a generalization to the local power law fit to account for changes in the curvature [3]. Using a polynomial of degree two to fit the logarithm of the MSD, the authors propose an

empirical localized version of (64) to be

$$(68) \quad \text{Dasgupta [3]:} \quad \tilde{G}_r(s) \approx \frac{2k_B T}{6\pi a s M(1/s)\Gamma(1 + \alpha(1/s))(1 + \beta(1/s)/2)}.$$

Further modified versions of the loss and storage forms (66) are proposed based on a degree two logarithmic fit of $\tilde{G}_r(s)$. However, for MSD that exhibits multiple time scales but transitions smoothly between the different regimes, this method has the same shortcoming as the local power law fit and does not provide any new information. For illustrative purposes, the reconstruction is given in Figure 22c.

3.3. Generalized Rouse Spectrum Identifiability Issues: $\tilde{G}_r(s) \longleftrightarrow G^*(\omega)$. Uncertainty arises from multiple sources in standard practice for passive microrheology. Some are experimental, like limitations on the camera frame rate ($1/\delta$) and the length of the particle paths (N_T). The conversion from the time domain to frequency space also introduces potential for error that we explore in the next section. In this section, we investigate parameter uncertainty that arises from the Rouse spectrum model itself: namely, while there are no pairs of unidentifiable parameters, there is a strong relationship between the parameters when an error is made. However, the effect on the inferred storage and loss moduli is relatively limited.

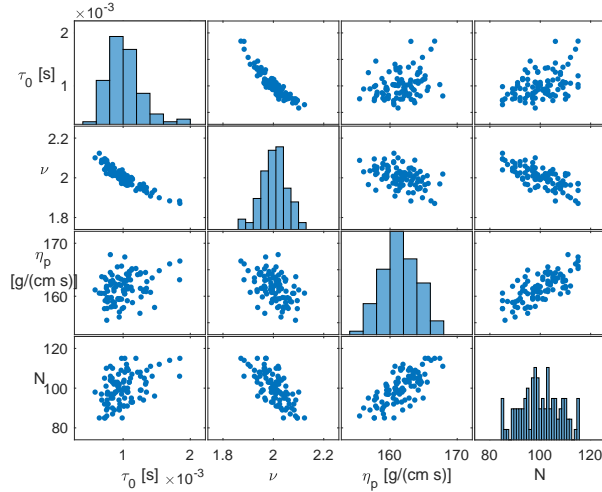


FIG. 3. PARAMETER RELATIONSHIPS FOR GENERALIZED ROUSE SPECTRUM MODEL. For a fixed parameter set, the corresponding function $\tilde{G}_r(s)$ was perturbed 100 times and estimated values for N, τ_0, η_p, ν were computed according to the procedure described in Eq. (70). Histograms of the values are plotted on the diagonal subplots, while scatter plots of each two parameters combination are on the off-diagonal. The scatter plots show that (τ_0, ν) are highly correlated, while none of the other parameters are. ($N = 100, \tau_0 = 10^{-3} \text{ s}, \eta_s = 10^{-2} \text{ g/(cm s)}, \eta_p/\tau_{avg} = 10^3 \text{ g/(cm s}^2\text{)}$.)

To assess the impact of what is sometimes called *practical unidentifiability* [31] among the parameters of the Generalized Rouse Spectrum, we conducted a numerical experiment in the spirit of the analysis carried out for cholera transmission pathways by Eisenberg et al [4]. Centered around the true value of the relaxation modulus $\tilde{G}_r(s)$, we generated 100 sets of randomly perturbed relaxation moduli. Following the procedure described below, for each perturbed version of $\tilde{G}_r(s)$, we conducted parameter estimation for N, η_p, τ_0 , and ν . In Figure 3, we plotted the histograms of

the estimated parameters on the diagonal as well as the scatter plots of two sets of estimated parameters on the off-diagonal subplot. When two parameters are highly correlated, then their estimated values lie on a curve in the scatter plot. This was the case for (τ_0, ν) (first row second plot, second row, first plot), but for none of the other groups. For each parameter quartet we plotted the coordinate pair (τ_0, ν) as a colored dot in Figure 4b and calculated the associated G' and G'' to be displayed as gray curves in Figure 4c. To explain our approach to generating these figures, we recall from (16), $\tilde{G}_r(s) = \eta_s + \frac{\eta_p}{\|K^+\|_1} \tilde{K}^+(s)$. When $K \in \mathcal{K}_{\text{Rouse}}$, this takes the form

$$(69) \quad \tilde{G}_r(s) = \eta_s + \frac{\eta_p}{\langle \tau_n \rangle} \frac{1}{N} \sum_{n=1}^N \frac{1}{s\tau_0 N^\nu + n^\nu}.$$

We generated 100 sets of T_N target pairs (s_i, \tilde{g}_i) , $i \in \{1, 2, \dots, T_N\}$. Each s_i is the inverse of a data observation time point t_i . We set the corresponding \tilde{g}_i value to be $\tilde{g}_i := \tilde{G}_r(s_i) + (0.1\tilde{G}_r(s_i))^{1/2}\epsilon_i$, where ϵ_i is a standard Normal random variable.

We then obtained a joint estimate for (η_p, N, τ_0, ν) by computing a solution to the least square fitting problem given by (69), assuming that η_s is known a priori. To be precise, for each N in a reasonable range, we numerically computed the parameter triplet (η_p, τ_0, ν) that minimized the residual function

$$(70) \quad R_N(\{\tilde{g}_i\}; \eta_p, \tau_0, \nu) := \sum_i \frac{(\tilde{g}_i - \tilde{G}_r(s_i; N, \eta_p, \tau_0, \nu))^2}{\tilde{g}_i^2}.$$

In practice, this was accomplished using the least square nonlinear fit command in Matlab. The optimization is constrained below by $\eta_p, \tau_0 \geq 0$ and $\nu \geq 1$. For the numerical experiment associated with Figure 4, we set the true parameters to be $N = 100$, $\eta_s = 10^{-2} \text{g}/(\text{cm s})$ corresponding to water, $\eta_p/\tau_{\text{avg}} = 10^3 \text{g}/(\text{cm s}^2)$ corresponding to $\eta_p \approx 163.5 \text{g}/(\text{cm s})$, $\tau_0 = 10^{-3} \text{s}$ and $\nu = 2$.

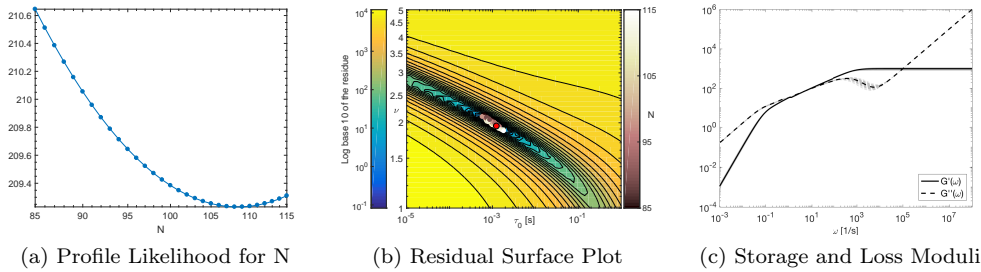


FIG. 4. GENERALIZED ROUSE SPECTRUM: UNCERTAINTY DUE TO $\tilde{G}_r(s) \longleftrightarrow G^*(\omega)$. For a fixed parameter set, the corresponding function $\tilde{G}_r(s)$ was perturbed 100 times and converted to $G'(\omega)$ and $G''(\omega)$ according to the procedure described in Section 3.3. In the **left panel**, a profile likelihood is provided for N for one of the 100 perturbations. In the **middle panel**, for each (τ_0, ν) pair, the color corresponds to the minimum possible residual from the true $\tilde{G}_r(s)$ among all admissible values for N and η_p . Each white dot corresponds to a parameter combination inferred for one perturbation of the true $\tilde{G}_r(s)$. These collect in a “trough” of the residual map. In the **right panel**, we see G' and G'' computed for all 100 of the perturbations. ($N = 100$, $\tau_0 = 10^{-3} \text{s}$, $\eta_s = 10^{-2} \text{g}/(\text{cm s})$, $\eta_p/\tau_{\text{avg}} = 10^3 \text{g}/(\text{cm s}^2)$.)

For notational efficiency, we will suppress dependence on the g_i and write

$$(71) \quad R_N^{\min}(\eta_p, \tau_0, \nu) := \min_{(\eta_p, \tau_0, \nu)} R_N(\{\tilde{g}_i\}; \eta_p, \tau_0, \nu).$$

It is important to observe that an error in the estimate of one parameter can be “compensated for” by a correlated error in the estimate of another parameter. One way to demonstrate this is through a *profile likelihood* plot, as in Figure 4a. For one instance of a perturbed set of target points $\{s_i, \tilde{g}_i\}$, we plotted $\log_{10} R_N^{\min}(\eta_p, \tau_0, \nu)$ as a function of $N \in \{85, \dots, 115\}$. We observe that there is a minimum point at $N \approx 107$ indicating that N can be reasonably estimated. However, the \log_{10} -residues vary only over a range of two units (from 209.4 to 210.6).

One way to visualize the relationship among the parameters is through a *residual heat map*, as seen for τ_0 and η_p in Figure 4b. For each (τ_0, η_p) pair in the displayed region, we found the combination of N and ν that minimized the residual function 70 and displayed the (τ_0, η_p) -minimal residual value in terms of colors ranging from blue (smallest residual) to yellow (relatively large residual). The presence of the blue-green “residual trough” indicates a region of (τ_0, η_p) that can provide similarly effective fits. Each white dot corresponds to a (N, η_p, τ_0, ν) combination that provided an optimal fit to a randomly perturbed version of the true $\tilde{G}_r(s)$. The red dot is the parameter combination corresponding to the minimal point in Figure 4a. We emphasize that the trough does indeed tend to capture the manner in which an error in one parameter will be compensated by a specific error in another parameter.

The essential observation in this numerical experiment is demonstrated in Figure 4c. Despite practical unidentifiability among the parameters, the inferred storage and loss moduli are quite consistent for a certain range of frequency ω . In the panel, the true $G'(\omega)$ and $G''(\omega)$ in black and overlay in gray the 100 $G'(\omega)$ and $G''(\omega)$ curves each corresponding to one of the parameter combinations associated with the white dots in Figure 4b. There is essentially no variation in the storage modulus G' is near the non-monotonic region that which appears in the range $\omega \in (10^2, 10^4) \text{ s}^{-1}$. We note that this non-monotonic his feature was studied in the single mode case by Marvin and Oser [22, 29], but we do not know of any analysis that exists when there are more Maxwell elements.

3.4. Converting time domain information the frequency domain. While the work in the previous section demonstrates identifiability issues that are intrinsic to the Generalized Rouse model for viscoelastic diffusion, a larger source of uncertainty lies in the conversion of path data to a quantity on which one can find optimal paramter sets, i.e. the connection $M(t) \longleftrightarrow \tilde{G}_r(s)$. As we have described above, Mason & Weitz were the first among many other who chose to compute a numerical Laplace transform of the MSD and use (25) to create an approximation of $\tilde{G}_r(s)$ on which to perform inference. In principle, one could perform the parameter optimization directly on the MSD. In Lemma 3.3 we provide a formula for the MSD in terms of $\hat{\rho}(\omega)$. For each parameter combination, it is trivial to compute $\hat{\rho}(\omega)$, however, we found that in practice, the numerical computation of Equation 72 is subject to extremely large numerical error. Some discussion concerning the computation of such an integral is provided in [12, 11, 10].

LEMMA 3.3. *Let $\{(X(t), V(t))\}_{t \geq 0}$ be defined as in Theorem 2.4. Then*

$$(72) \quad M(t) = \frac{4}{\pi} \int_0^\infty \sin^2\left(\frac{t\omega}{2}\right) \frac{\hat{\rho}(\omega)}{\omega^2} d\omega.$$

Proof. Recalling that $\rho(t) = \mathbb{E}(V(t)V(0))$ and using the definition of $M(t)$, we have $M(t) = \int_0^t \int_0^t \rho(s - s') ds' ds$. Next, expressing $\rho(s - s')$ in terms of its Fourier

inverse transform gives

$$(73) \quad M(t) = \int_0^t \int_0^t \frac{1}{2\pi} \int_{-\infty}^{\infty} e^{-i(s-s')\omega} \hat{\rho}(\omega) d\omega ds' ds.$$

The claim follows by switching the order of integration in (73), integrating, using the Euler's formula and the fact that $\hat{\rho}(\omega)$. \square

Computing a numerical Laplace transform presents its own problems. The first, and most prominent, is that because the MSD of a particle is an increasing function, the tail of the integrand of the Laplace Transform is not trivial. As is also pointed out in Evans et al [5], it is necessary to project behavior of the MSD for regions outside of the values given by the data. We suppose the observations are taken over a time interval $t \in [t_1, T]$ which is divided into equally spaced subintervals with observations at the times $t_i := i\Delta t$, $i = 1, \dots, N_T$. For each i , we write $M_i := M(t_i)$.

It is natural to split the Laplace transform into three regions:

$$(74) \quad \begin{aligned} \widetilde{M}(s) &= I_1(s) + I_2(s) + I_3(s) \\ &:= \int_0^{t_1} e^{-st} M(t) dt + \int_{t_1}^T e^{-st} M(t) dt + \int_T^{\infty} e^{-st} M(t) dt. \end{aligned}$$

To approximate $I_2(s)$ it is sufficient to use the trapezoidal rule:

$$(75) \quad \int_{t_1}^T e^{-st} M(t) dt \approx \widetilde{M}_{\text{trap}}(s) = \frac{\Delta t}{2} \sum_{j=1}^{N_T-1} (e^{-st_{j+1}} M(t_{j+1}) + e^{-st_j} M(t_j)).$$

On the intervals $[0, t_1]$ and $[T, \infty)$, we approximate $M(t)$ by $C_0 t^{q_0}$ and by $C_{\infty} t^{q_{\infty}}$ respectively, where the coefficients and exponents are obtained by linearly fitting a small number of points on the beginning and on the tail of $\ln M(t)$ to $\ln t$. In practice, we assume that there are 2048 time points for which the particle position is observed. The ensemble pathwise MSD is very noisy for large time, so it is standard practice to only use the first 10% to 20% of the time points. We therefore set the number of target points to be $N_T = 200$ to find the coefficients.

Outside of the observed range, the approximations simplify to

$$(76) \quad \begin{aligned} \int_0^{t_1} e^{-st} M(t) dt &\approx \frac{C_0}{s^{q_0+1}} \gamma(st_1, q_0 + 1) \text{ and} \\ \int_T^{\infty} e^{-st} M(t) dt &\approx \frac{C_{\infty}}{s^{q_{\infty}+1}} \Gamma(sT, q_{\infty} + 1), \end{aligned}$$

where $\gamma(a, x) = \int_0^x t^{a-1} e^{-t} dt$ is the lower incomplete Gamma function and $\Gamma(a, x) = \int_x^{\infty} t^{a-1} e^{-t} dt$ is the upper incomplete Gamma function. Combining (74)-(76), we have

$$(77) \quad \widetilde{M}(s) \approx \widetilde{M}_{\text{app}}(s) = \frac{C_0}{s^{q_0+1}} \gamma(st_1, q_0 + 1) + \widetilde{M}_{\text{trap}}(s) + \frac{C_{\infty}}{s^{q_{\infty}+1}} \Gamma(sT, q_{\infty} + 1).$$

In order to visualize the increased uncertainty that arises from (1) only being able to observe the MSD at a small number of time points, and (2) needing to compute a numerical Laplace transform, we generated a second residual heat map (Figure 5a. For the given set of 200 time points $\{t_1, t_2, \dots, T\}$ we generated an associated set of

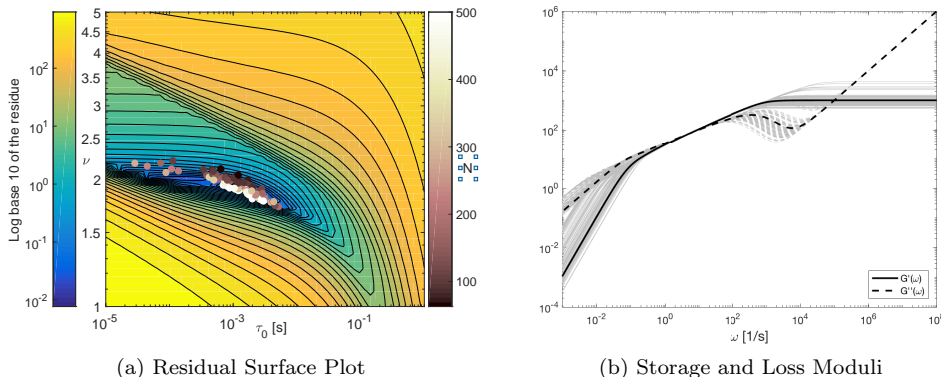


FIG. 5. MONTE CARLO VISUALIZATION OF THE FULL METHOD: $\mathcal{M}(t) \longleftrightarrow M(t) \longleftrightarrow \tilde{G}_r(s) \longleftrightarrow G^*(\omega)$. For the same baseline parameter set used for Figure 4, we assess uncertainty that arises due to computing an ensemble MSD from simulated data, converting this estimate for the true MSD to an estimate for $\tilde{G}_r(s)$ and finding an optimal parameter fit. In the **left panel**, for each (τ_0, ν) pair, the color corresponds to the minimum possible residual from the true $\tilde{G}_r(s)$ among all admissible values for N and η_p . One hundred (τ_0, ν) pairs were chosen from the trough in the residual map and the color corresponds to the value of N that gave the smallest residual value. In the **right panel**, we see G' and G'' computed for all 100 (τ_0, ν) pair displayed in the middle panel.

target points (s_i, \tilde{g}_i) . For each $i \in \{1, \dots, N_T\}$, we set $s_i = t_i^{-1}$ and then used (77) to compute $\tilde{M}_{\text{app}}(s_i)$. Then corresponding estimate \tilde{g}_i for $\tilde{G}_r(s_i)$ was computed by way of Equation 25 in Theorem 2.4:

$$(78) \quad \tilde{g}_i := \frac{1}{6\pi a} \left[\frac{2c}{s_i^2 \tilde{M}_{\text{app}}(s_i)} - m s_i \right].$$

As with Figure 4b, the color coding reveals which combinations of τ_0 and ν can be combined with optimal values of N and η_p to yield a function $\tilde{G}_r(s; N, \eta_p, \tau_0, \nu)$ that is close to the target values at the frequencies $\{s_i\}$. However, for Figure 5a (and Figure 6a) we introduced a weighted residual function. The reason for the weights is that every \tilde{g}_i value has a contribution from each of $I_1(s_j)$, $I_2(s_j)$ and $I_3(s_j)$ in (74). Importantly, points nearer the boundary of the observation window have larger contributions from I_1 and I_3 which contain the projected information. Moreover, there reasonable disagreement concerning what is an appropriate projection into the large- t region ($t > T$). As demonstrated by Theorem 2.3, when there are finitely many terms in the Prony series, the sublinear character of the MSD only exists over a finite range. So, eventually the MSD will grow linearly. The question is whether the linear regime will emerge shortly after the observable time range, whether the present power law behavior near time $t = T$ will persist. We have chosen to project the sublinear behavior to all $t > T$, and this is the choice effectively made by the methods adopted by Mason [24] and Dasgupta et al. [3]. However, Evans et al. [5] opted to project into the large- t region with linear growth.

The residuals used in this section are therefore computed with the weights $w_i := I_2(s_i)/\tilde{M}(s_i)$. In this way, w_i is the fraction of the value \tilde{g}_i that is given by non-

projected data points. Then

$$(79) \quad R_N(\eta_p, \tau_0, \nu; w) := \sum_{i=1}^{N_T} w_i^2 \frac{(\tilde{g}_i - \tilde{G}_r(s_i))^2}{\tilde{g}_i^2}.$$

Note that, as a result of the relatively small number of observed time points and the numerical computation of the Laplace transform, the blue trough of (τ_0, ν) pairs that can be part of “good-fitting quartets” (N, τ_0, ν, η_p) is much larger. As we discuss in the next section, this trough structure captures the shape of the best fit parameter sets for simulated data.

3.5. Monte Carlo Visualization of Uncertainty in the Storage and Loss Moduli. We use numerical simulation to portray our final assessment of uncertainty the *passive microrheology* procedure. Using a covariance-based algorithm to generate GLE paths (described in [10, 12, 11]), mimic experimental conditions, taking $\Delta t = 2^{-2}\text{s}$, $N_T = 2048$ and $N_P = 75$ (number of paths). To construct $\mathcal{M}(t)$, for each path we computed a pathwise MSD, defined as in (11). Then our estimated for the MSD, $M(t)$ was the ensemble average of pathwise MSDs. For our observation times, we chose $t_i = i\Delta t$, for $i \in \{1, \dots, 200\}$. Given this collection of MSD estimates, we computed the target points (s_i, \tilde{g}_i) as described in the previous section and found the parameter set that minimized the weighted residual function 79.

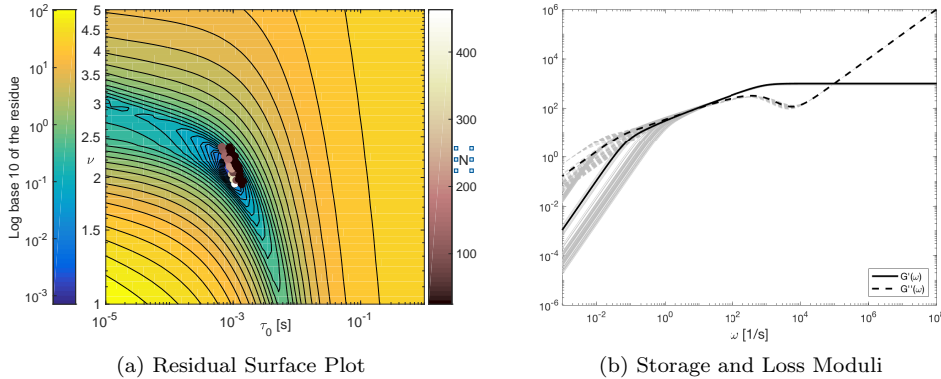


FIG. 6. ASSESSING THE EFFECT OF A 100X FASTER FRAME RATE. For the same baseline parameter set used in the previous figures, we repeat the procedure applied to create Figure 5, but shifted the observation times down by a factor of 100. We see that the parameter τ_0 can be much better estimated; however there is greater uncertainty regarding ν and N . (Uncertainty for N , not pictured.)

Each dot in Figure 5a corresponds to a (τ_0, ν) pair that produced an optimal fit for a given path. The color of each dot indicates the associated value of N in the optimal quartet. From the figure, we see that the estimates for N and τ_0 in particular are quite noisy. However, despite this uncertainty in parameter estimation, the inference for a certain range of the storage and loss moduli is very tight. Indeed, in Figure 5b the gray curves represent the Storage (G' , solid) and Loss (G'' , loss) moduli associated with each parameter quartet fit.

In Figure 6, we carried out the same procedure for the same parameter set, but then supposed that the experimental camera frame rate is 100 times as fast (but we

assume that the movies have the same number of total frames, so we lose observations for larger t). It is interesting to see the change in shape of the blue residual trough. The improved frame rate allows the parametrization to “rule out” the range of τ_0 values $[2 \times 10^{-3} s, 10^{-1} s]$, which were plausible before. Because the range of τ_0 is narrowed, the range of N values is diminished as well. For the storage and loss moduli, the range of ω -values that have good certainty have shifted right, as expected, including the Oser & Marvin feature. In fact, because the estimate for η_p improved considerably, the range of certainty extends well beyond the experimental time scale in the high frequency range.

4. Discussion. Biological fluids, like mucus and the cytoplasm of cells, exhibit a wide range of viscoelastic properties that are essentially impossible to study by traditional rheological techniques. Because fluid samples are intrinsically small and difficult to collect, *microrheological* tools, which rely on studying the fluctuating behavior of immersed microparticles, have become indispensable. The fundamental challenge for these inference methods though, is that while the data is collected in the time domain, the standard characterizations of viscoelastic fluids are articulated in Fourier frequency space. In this work, we have put the fundamental assumptions of what is sometimes called the Mason & Weitz protocol on rigorous footing and attempted to quantify the uncertainty that is introduced in each step of the procedure.

According to the Mason & Weitz hypothesis, the behavior of a particle immersed in a complex fluid is well-described by the Generalized Langevin Equation that has a memory kernel that matches the fluid’s shear relaxation modulus $G_r(t)$. We accepted this premise as true throughout this work and focused on the problem of inferring the Laplace transform of $G_r(t)$ from particle position data, which can then be related to $G'(\omega)$ and $G''(\omega)$ by analytic continuation. Mason & Weitz proposed a relationship between a particle’s Mean-Squared Displacement and its memory kernel (Equation 25), but to our knowledge this formula had never been established rigorously before now (Theorem 2.4). In fact, the justification for this formula is usually provided by an assumption that turns out not to be true at all!

The issue is that the model that appears in the physics literature is not properly stated. Although it suffices to specify the initial condition of the position process to be $X(0) = 0$, because the velocity process satisfies a stochastic *integro*-differential equation, one must specify the entire past $\{V(t)\}_{t \leq 0}$. Either this, or through use of a Mori-Zwanzig apparatus, one can define statistically equivalent dynamics by way of a system of auxiliary variables $(Z_n(t))$ (either by (26) or (36)). In this case, the history of V is captured by the collection of initial values for the auxiliary terms. Taking the definition in the physics literature literally is equivalent of assuming that $Z_n(0) = 0$ in the system (36). In order to justify the Mason & Weitz relationship 25, for over fifty years dating back to Kubo [16], authors have assumed that $\mathbb{E}(F(t)V(0)) = 0$. We have proved that this is not the case, Theorem 2.5. Remarkably, these observations do not disrupt the veracity of the Mason & Weitz formula, Theorem 2.4.

Having established confidence in the Mason & Weitz formula, we proceeded to analyze the inversion procedure itself: reconstructing $G'(\omega)$ and $G''(\omega)$ from particle path data. There have been attempts to do this with a non-parametric approach, but as we argue in Section 3.4, and as has been observed elsewhere [5], any procedure that involves numerically relating Mean-Squared Displacement (MSD) of the position process to the Autocovariance Function (ACF) of the velocity process will require projecting MSD values beyond the experimentally observed time range. By way of the small- and large- ω asymptotics for $G'(\omega)$ and $G''(\omega)$ that we studied in Section

3.1, we can argue that the MSD projection will dominate both ω extremes. In other words, the inferred $G'(\omega)$ and $G''(\omega)$ for small- and large- ω will depend more on the project technique than the actual process, which contradicts the point of using a non-parametric method in the first place. We therefore adopted a form for $G_r(t)$, (18), that is well-established in polymer physics literature [6]. Moreover, we used a tunable four-parameter family of functions (2.1) for which the GLE can mimic a wide array of experimentally observed behavior [26]. We note that there are other methods for parametrizing Prony series kernels to produce similar behavior, see [17, 14] for example, but we reserve for future work an investigation of what happens when one parametric family is used for inference on a GLE generated by another family.

As seen in Section 3.4, even when the correct parametric family is used for reconstruction, there is considerable error introduced by (1) the constraint of finite time series observations; and (2) the conversion time domain information to Fourier frequency space. The error is not uniform in ω though. While we were reluctant to use the precise language of confidence intervals and hypothesis testing (because there are some ambiguities how such statistical tests should be set up), we introduced a Monte Carlo visualization of the uncertainty intrinsic to passive microrheology. We have showed that, while there can be significant uncertainty in the estimation of certain parameters (in particular, the smallest relaxation time τ_0 and the number of distinct linear relaxation times N , Figures 4b, 5a and 6a) there is remarkable consistency in the inferred values for $G'(\omega)$ and $G''(\omega)$ over the range of frequencies that correspond to experimentally observed times (Figures 4c, 5b, and 6b).

This observation is very much in the spirit of many Uncertainty Quantification investigations that show that parameter estimation should not be an end in and of itself. Often, parameters values are useful only to the extent that they help produce some scientifically relevant prediction. When a methodology is sound, as the protocol used for passive microrheology seems to be, the prediction of interest (in our case, characterization of the storage and loss moduli) is robust and stable despite the potential for large error in parameter estimation.

Acknowledgements. The authors thank Hung Nguyen, Gustavo Didier, and Marisa Eisenberg for fruitful conversations in the development of this work.

REFERENCES

- [1] D. CHEN, A. LAU, L. HOUGH, M. ISLAM, M. GOULIAN, T. LUBENSKY, AND A. YODH, *Fluctuations and Rheology in Active Bacterial Suspensions*, Physical Review Letters, 99 (2007).
- [2] J. CROCKER, M. VALENTINE, E. WEEKS, T. GISLER, P. KAPLAN, A. YODH, AND D. WEITZ, *Two-Point Microrheology of Inhomogeneous Soft Materials*, Physical Review Letters, 85 (2000), pp. 888–891.
- [3] B. R. DASGUPTA, S.-Y. TEE, J. C. CROCKER, B. J. FRISKEN, AND D. A. WEITZ, *Microrheology of polyethylene oxide using diffusing wave spectroscopy and single scattering*, Physical Review E, 65 (2002), p. 051505.
- [4] M. C. EISENBERG, S. L. ROBERTSON, AND J. H. TIEN, *Identifiability and estimation of multiple transmission pathways in cholera and waterborne disease*, Journal of Theoretical Biology, (2013).
- [5] R. EVANS, M. TASSIERI, D. AUHL, AND T. A. WAIGH, *Direct conversion of rheological compliance measurements into storage and loss moduli*, Physical Review E, 80 (2009), p. 012501.
- [6] J. D. FERRY, *Viscoelastic properties of polymers*, John Wiley & Sons, 1980.
- [7] J. FRICKS, L. Y. YAO, T. C. ELSTON, AND M. G. FOREST, *Time domain methods for passive microrheology and anomalous diffusive transport in soft matter*, SIAM Journal of Applied Math, 69 (2009), pp. 1277–1308.
- [8] M. GRIMM, S. JENEY, AND T. FRANOSCH, *Brownian motion in a Maxwell fluid*, Soft Matter, 7 (2011), pp. 2076–2084.

- [9] D. B. HILL, P. A. VASQUEZ, J. MELLNIK, S. A. MCKINLEY, A. VOSE, F. MU, A. G. HENDERSON, S. H. DONALDSON, N. E. ALEXIS, R. C. BOUCHER, AND M. G. FOREST, *A Biophysical Basis for Mucus Solids Concentration as a Candidate Biomarker for Airways Disease*, PLoS ONE, 9 (2014), p. e87681.
- [10] C. HOHENEGGER, *On equipartition of energy and integrals of Generalized Langevin Equations with generalized Rouse kernel*, Communications in Mathematical Sciences, 15 (2017), pp. 539–554.
- [11] C. HOHENEGGER, R. DURR, AND D. M. SENTER, *Mean first passage time in a thermally fluctuating viscoelastic fluid*, Journal of Non-Newtonian Fluid Mechanics, 242 (2017), pp. 48–56.
- [12] C. HOHENEGGER AND S. A. MCKINLEY, *Fluid-particle dynamics for passive tracers advected by a thermally fluctuating viscoelastic medium*, Journal of Computational Physics, 340 (2017), pp. 688–711.
- [13] T. INDEI, J. D. SCHIEBER, A. CÓRDOBA, AND E. PILYUGINA, *Treating inertia in passive microbead rheology*, Physical Review E, 85 (2012), p. 021504.
- [14] S. C. KOU, *Stochastic modeling in nanoscale biophysics: subdiffusion within proteins*, The Annals of Applied Statistics, (2008), pp. 501–535.
- [15] R. KUBO, *Statistical Mechanics*, Elsevier, 1965.
- [16] R. KUBO, *The fluctuation-dissipation theorem*, Reports on progress in physics, 29 (1966), p. 255.
- [17] R. KUPFERMAN, *Fractional kinetics in kac-zwanzig heat bath models*, Journal of statistical physics, 114 (2004), pp. 291–326.
- [18] S. K. LAI, Y.-Y. WANG, D. WIRTZ, AND J. HANES, *Micro-and macrorheology of mucus*, Advanced Drug Delivery Reviews, 61 (2009), pp. 86–100.
- [19] W. LAI, S. KUEI, AND V. MOW, *Rheological equations for synovial fluids*, Journal of Biomechanical Engineering, 100 (1978), p. 169.
- [20] R. G. LARSON, *Constitutive Equations for Polymer Melts and Solutions*, Butterworth-Heinemann, 1988.
- [21] A. J. LEVINE AND T. C. LUBENSKY, *One-and two-particle microrheology*, Physical Review Letters, 85 (2000), pp. 1774–1777.
- [22] R. S. MARVIN AND H. OSER, *A model for the viscoelastic behavior of rubberlike polymers including entanglements effects*, J Res Natl Bur Stand B, 66 (1962), pp. 171–180.
- [23] T. MASON AND D. WEITZ, *Optical measurements of frequency-dependent linear viscoelastic moduli of complex fluids*, Physical Review Letters, 74 (1995), pp. 1250–1253.
- [24] T. G. MASON, *Estimating the viscoelastic moduli of complex fluids using the generalized Stokes-Einstein equation*, Rheologica Acta, 39 (2000), pp. 371–378.
- [25] G. MASSIERA, K. M. VAN CITTERS, P. L. BIANCANIELLO, AND J. C. CROCKER, *Mechanics of single cells: rheology, time dependence, and fluctuations*, Biophysical Journal, 93 (2007), pp. 3703–3713.
- [26] S. A. MCKINLEY, L. YAO, AND M. G. FOREST, *Transient anomalous diffusion of tracer particles in soft matter*, Journal of Rheology, 53 (2009), pp. 1487–1506.
- [27] H. MORI, *Transport, collective motion, and brownian motion*, Progress of Theoretical Physics, 33 (1965), pp. 423–455.
- [28] H. NGUYEN AND S. A. MCKINLEY, *Anomalous diffusion and the generalized langevin equation*. In preparation. (We note that the work presented in this submission does not depend on the results stated in these theorems. We provide these statements for context.), 2017.
- [29] H. OSER AND R. S. MARVIN, *Effect of molecular weight on viscoelastic properties of polymers as predicted by a molecular theory*, J. Res. Nat. Bur. Stand. B, 67 (1963), pp. 87–90.
- [30] G. A. PAVLIOTIS, *Stochastic Processes and Applications*, Springer, 2014.
- [31] A. RAUE, C. KREUTZ, T. MAIWALD, J. BACHMANN, M. SCHILLING, U. KLINGMÜLLER, AND J. TIMMER, *Structural and practical identifiability analysis of partially observed dynamical models by exploiting the profile likelihood*, Bioinformatics, 25 (2009), pp. 1923–1929.
- [32] F. REIF, *Fundamentals of Statistical and Thermal Physics*, Waveland Press, 1965.
- [33] T. M. SQUIRES AND T. G. MASON, *Fluid Mechanics of Microrheology*, Annual Review of Fluid Mechanics, 42 (2010), pp. 413–438.
- [34] L. STARRS AND P. BARTLETT, *One- and two-point micro-rheology of viscoelastic media*, Journal of Physics: Condensed Matter, 15 (2002), pp. S251–S256.
- [35] M. T. VALENTINE, Z. E. PERLMAN, M. L. GARDEL, J. H. SHIN, P. MATSUDAIRA, T. J. MITCHISON, AND D. A. WEITZ, *Colloid surface chemistry critically affects multiple particle tracking measurements of biomaterials*, Biophysical journal, 86 (2004), pp. 4004–4014.
- [36] R. ZWANZIG, *Nonlinear generalized langevin equations*, Journal of Statistical Physics, 9 (1973), pp. 215–220.
- [37] R. ZWANZIG AND M. BIXON, *Hydrodynamic theory of the velocity correlation function*, Phys. Rev. A, 2 (1970), pp. 2005–2012.